Phosphatidylinositol-(4,5)-bisphosphate regulates clathrin-coated pit initiation, stabilization, and size

Costin N. Antonescu[a], François Aguet[b], Gaudenz Danuser[b], and Sandra L. Schmid[a]
[a]Department of Cell Biology, The Scripps Research Institute, La Jolla, CA 92037; [b]Department of Cell Biology, Harvard Medical School, Boston, MA 02115

ABSTRACT **Clathrin-mediated endocytosis (CME) is the major mechanism for internalization in mammalian cells. CME initiates by recruitment of adaptors and clathrin to form clathrin-coated pits (CCPs). Nearly half of nascent CCPs abort, whereas others are stabilized by unknown mechanisms and undergo further maturation before pinching off to form clathrin-coated vesicles (CCVs). Phosphatidylinositol-(4,5)-bisphosphate (PIP_2), the main lipid binding partner of endocytic proteins, is required for CCP assembly, but little is currently known about its contribution(s) to later events in CCV formation. Using small interfering RNA (siRNA) knockdown and overexpression, we have analyzed the effects of manipulating PIP_2 synthesis and turnover on CME by quantitative total internal reflection fluorescence microscopy and computational analysis. Phosphatidylinositol-4-phosphate-5-kinase cannot be detected within CCPs but functions in initiation and controls the rate and extent of CCP growth. In contrast, the 5′-inositol phosphatase synaptojanin 1 localizes to CCPs and controls early stabilization and maturation efficiency. Together these results suggest that the balance of PIP_2 synthesis in the bulk plasma membrane and its local turnover within CCPs control multiple stages of CCV formation.**

Monitoring Editor
Jean E. Gruenberg
University of Geneva

Received: Apr 26, 2011
Revised: May 10, 2011
Accepted: May 17, 2011

INTRODUCTION

Clathrin-mediated endocytosis (CME) is the major pathway for internalization of receptor-bound macromolecules (i.e., cargo) from the surface of mammalian cells. In a multistep process, clathrin, cargo-binding adaptors (e.g., Adaptor Protein 2 [AP-2]), and numerous endocytic accessory proteins (EAPs) assemble at the plasma membrane (PM) into invaginating clathrin-coated pits (CCPs) (Slepnev and De Camilli, 2000; Conner and Schmid, 2003; Traub, 2003). Nearly half of nascent CCPs quickly turn over (so-called abortive events), whereas others are stabilized, undergo a maturation process, and pinch off to form clathrin-coated vesicles (CCVs) (Ehrlich *et al.*, 2004; Loerke *et al.*, 2009).

Recently we proposed that CCP maturation is gated by an endocytic checkpoint (Loerke *et al.*, 2009; Mettlen *et al.*, 2009, 2010). According to this hypothesis, nascent CCPs must be stabilized by recruitment of adaptors, cargo, and other EAPs to prevent coat disassembly and abortive turnover. Nascent CCPs with sufficient stability progress to a maturation stage leading to eventual closing of CCPs and scission of CCVs. Using small interfering RNA (siRNA)-mediated knockdown and dual-label total internal reflection fluorescence (TIRF) microscopy, we and others have begun to establish a temporal hierarchy of functional requirements of EAPs in CCP initiation, stabilization, and maturation (Merrifield *et al.*, 2005; Rappoport *et al.*, 2006; Saffarian and Kirchhausen, 2008; Mettlen *et al.*, 2009; Loerke *et al.*, 2011; Taylor *et al.*, 2011).

Many proteins are recruited to CCPs in part via low-affinity interaction(s) with phosphatidylinositol-(4,5)-bisphosphate (PIP_2), including the AP-2 subunits α, β2, and μ2 (Gaidarov and Keen, 1999; Jackson *et al.*, 2010), SNX9 (Yarar *et al.*, 2007, 2008), epsin (Itoh *et al.*, 2001), CALM/AP180 (Ford *et al.*, 2001), Dab2 (Yun *et al.*, 2003), HIP1/HIP1R (Itoh *et al.*, 2001), and dynamin (Vallis *et al.*,

This article was published online ahead of print in MBoC in Press (http://www.molbiolcell.org/cgi/doi/10.1091/mbc.E11-04-0362) on May 25, 2011.

Address correspondence to: Sandra L. Schmid (slschmid@scripps.edu).

Abbreviations used: AP-2, Adaptor Protein 2; CCP, clathrin-coated pit; CCV, clathrin-coated vesicle; CHC, clathrin heavy chain; CME, clathrin-mediated endocytosis; EAP, endocytic accessory protein; EGF, epidermal growth factor; eGFP-CLC, enhanced green fluorescent protein fused to clathrin light chain; KD, kinase-dead; OCRL, Oculocerebrorenal Syndrome of Lowe; PD, 5′-inositol phosphatase-dead; PH, Pleckstrin Homology; PIP_2, phosphatidylinositol-(4,5)-bisphosphate; PIP5K, phosphatidylinositol-4-phosphate-5-kinase; PM, plasma membrane; SHIP2, SH2-domain-containing inositol 5′-phosphatase; Sjn, synaptojanin; SV, synaptic vesicle; tet, tetracycline; TfR, Tfn receptor; TIRF, total internal reflection fluorescence; Tfn, transferrin; WT, wild-type.

1999). These interactions contribute to a coincidence detection mechanism of PM and cargo proteins (Carlton and Cullen, 2005; Schmid and McMahon, 2007). The specific role, however, of PIP_2 during CCV formation has not been systematically addressed. Severe perturbation of PIP_2 by sequestration (Jost *et al.*, 1998) or recruitment of a 5′-inositol phosphatase to the PM (Malecz *et al.*, 2000; Zoncu *et al.*, 2007) ablated CCPs, establishing that PIP_2 is required for CCP initiation. A subsequent study, however, suggested that AP-2 recruitment might be more sensitive to PIP_2 levels than the recruitment of other adaptors and clathrin (Abe *et al.*, 2008). Although these studies have collectively established that PIP_2 is required for CME, because of the potent effects on CCP initiation, they were unable to address potential contributions of PIP_2 to nascent CCP stabilization and maturation. Understanding the role of PIP_2 in subsequent stages of CCV formation will require more subtle perturbations of PIP_2 levels and quantitative analyses of their effects on CCP dynamic behavior.

Three isoforms of type I phosphatidylinositol-4-phosphate-5-kinase (PIP5Kα, β, and γ) phosphorylate phosphatidylinositol-4-phosphate and are largely responsible for PIP_2 synthesis in mammalian cells (Doughman *et al.*, 2003). siRNA-mediated knockdown of PIP5Kβ decreased PIP_2 levels and reduced internalization of transferrin (Tfn), a well-studied cargo of CME (Padron *et al.*, 2003). Overexpression of PIP5Kα (Barbieri *et al.*, 2001) or PIP5Kβ (Padron *et al.*, 2003) increased internalization of epidermal growth factor (EGF) or Tfn, respectively. As PIP5Ks can bind to AP-2 (Bairstow *et al.*, 2006; Krauss *et al.*, 2006; Thieman *et al.*, 2009), it has been suggested that these interactions create a positive feedback mechanism for local synthesis of PIP_2 within assembling CCPs (Haucke, 2005). Despite the biochemical evidence of PIP5K interaction with endocytic proteins, however, specific recruitment of PIP5Ks to CCPs has not been demonstrated.

Paradoxically, although PIP_2 is important for CME, its turnover by 5′-dephosphorylation may occur locally within CCPs and also contribute to CCV formation. Several 5′-inositol phosphatases bind to CCP protein components, including SH2-domain-containing inositol 5′-phosphatase (SHIP2), which binds to intersectin (Nakatsu *et al.*, 2010), OCRLa (Oculocerebrorenal Syndrome of Lowe), which binds to clathrin and AP-2 and localizes to a subset of CCPs (Choudhury *et al.*, 2009; Mao *et al.*, 2009), and synaptojanin (Sjn) 1, which binds to clathrin, AP-2, and endophilin (Perera *et al.*, 2006) and localizes to CCPs throughout their lifetime (Perera *et al.*, 2006). Knockdown of the related Sjn2 impacts multiple stages of CCV formation (Rusk *et al.*, 2003), although its localization relative to CCPs has not been examined. Together these studies suggest that the temporal and spatial regulation of PIP_2 synthesis and turnover may function at multiple stages in CCV formation.

To further address the role(s) of PIP_2 synthesis and turnover in CCV formation, we have studied CME by tracking the dynamics of individual CCPs in live cells. This method couples time-lapse TIRF microscopy in cells expressing enhanced green fluorescent protein fused to clathrin light chain (eGFP-CLC) to computational tracking of CCPs and analysis of their lifetimes (Jaqaman *et al.*, 2008; Loerke *et al.*, 2009). With this approach, we have previously shown that CCPs exist in three dynamically distinct subpopulations: two short-lived subpopulations ($\tau < 20$–30 s), hypothesized to be abortive, and a longer-lived productive ($\tau = 30$–120 s) subpopulation leading to CCV formation (Loerke *et al.*, 2009; Mettlen *et al.*, 2009, 2010). The ratio of the abortive to productive pits reflects the stabilization of nascent CCPs and the efficiency of their maturation, whereas the lifetimes of productive CCPs reflect their rate of maturation leading to CCV scission. We have also used recently developed methods (Loerke *et al.*, 2011) to systematically and automatically measure the recruitment of lipid kinases and phosphatases to CCPs. Using these assays in conjunction with siRNA-mediated knockdown and protein overexpression of PIP5Ks and 5′-inositol phosphatases, we have examined the spatial regulation of PIP_2 synthesis and turnover and defined the spatiotemporal requirements for PIP_2 dynamics in CCP initiation, stabilization, growth, and maturation.

RESULTS

PIP_2 can be readily detected in the PM by the use of fluorescent probes such as the Pleckstrin Homology (PH) domain of phospholipase Cδ fused to mCherry (mCherry-PH). This approach has been used to reveal PIP_2 enrichment in larger structures such as sites of phagocytosis (Botelho *et al.*, 2000) and the cleavage furrows of dividing *Drosophila* spermatocytes (Wong *et al.*, 2005). We were unable, however, to detect enrichment within CCPs of either mCherry-PH or of a similar probe with tandem PH domains and hence increased PIP_2 affinity (unpublished data). We also did not detect enrichment of an mCherry fusion of the PIP_2-binding ANTH domain of CALM in CCPs (unpublished data), although in yeast a similar fusion with the ANTH domain of Sla2p was enriched in CCPs (Sun *et al.*, 2007). PIP_2 within or near CCPs, however, may be sequestered by its numerous endogenous binding proteins recruited to these sites and hence unavailable for detection (McLaughlin *et al.*, 2002; Catimel *et al.*, 2008). Therefore, instead of directly visualizing PIP_2, we manipulated the expression of the enzymes that mediate phosphoinositide phosphorylation/dephosphorylation (referred to here as PIP_2 synthesis and turnover, respectively) to indirectly probe the role of PIP_2 dynamics in CCP initiation, stabilization, and maturation.

PIP5K isoforms cannot be detected in CCPs

We first examined the dynamic distribution of mCherry-PIP5Ks (PIP5Kα, β, and γ) relative to CCPs by dual-color, time-lapse TIRF microscopy imaging of BSC-1 cells expressing eGFP-CLC (see Supplemental Movies 1–4 and representative single frames in Figure 1A). PIP5Kγ exhibits several splice variants; we used the 661 isoform that harbors all known possible AP-2 binding sites (Nakano-Kobayashi *et al.*, 2007; Thieman *et al.*, 2009; Kahlfeldt *et al.*, 2010). All three isoforms of PIP5K were enriched in the PM relative to cytosol as observed by fluorescence microscopy (unpublished data). Notably, PIP5Kγ, but not PIP5Kα or β, was readily seen in focal adhesions (Figure 1A), as previously described (Di Paolo *et al.*, 2002). Quantification of the fluorescence intensity of mCherry-PIP5K isoforms within CCP tracks ($n > 30{,}000$) revealed no enrichment of any of these lipid kinases in either short-lived or longer-lived CCPs, from 20 s before clathrin detection to 20 s following its disappearance from the TIRF field (Figure 1B). The lack of PIP5K recruitment to CCPs suggests that their binding interactions with CCP components are of low affinity and/or that their binding is prevented or rapidly displaced by competitive binding of other EAPs to AP-2. As PIP5Ks are not enriched within CCPs, PIP_2 synthesis must occur largely in the bulk PM.

Increased PIP_2 synthesis differentially affects the rates of CME and CCP assembly

We next used an adenovirus strategy for efficient tetracycline (tet)-regulated expression of exogenous proteins in BSC-1 cells (Loerke *et al.*, 2009; Liu *et al.*, 2010; Mettlen *et al.*, 2010) to express eGFP-PIP5Kα (wild-type [WT] or kinase-dead [KD]) in BSC-1 cells (Figure 2A) and examined its effects on CME. We found that, even at low levels of overexpression, PIP5Kα WT (but not KD) resulted in a small but significant decrease in Tfn internalization that was more pronounced

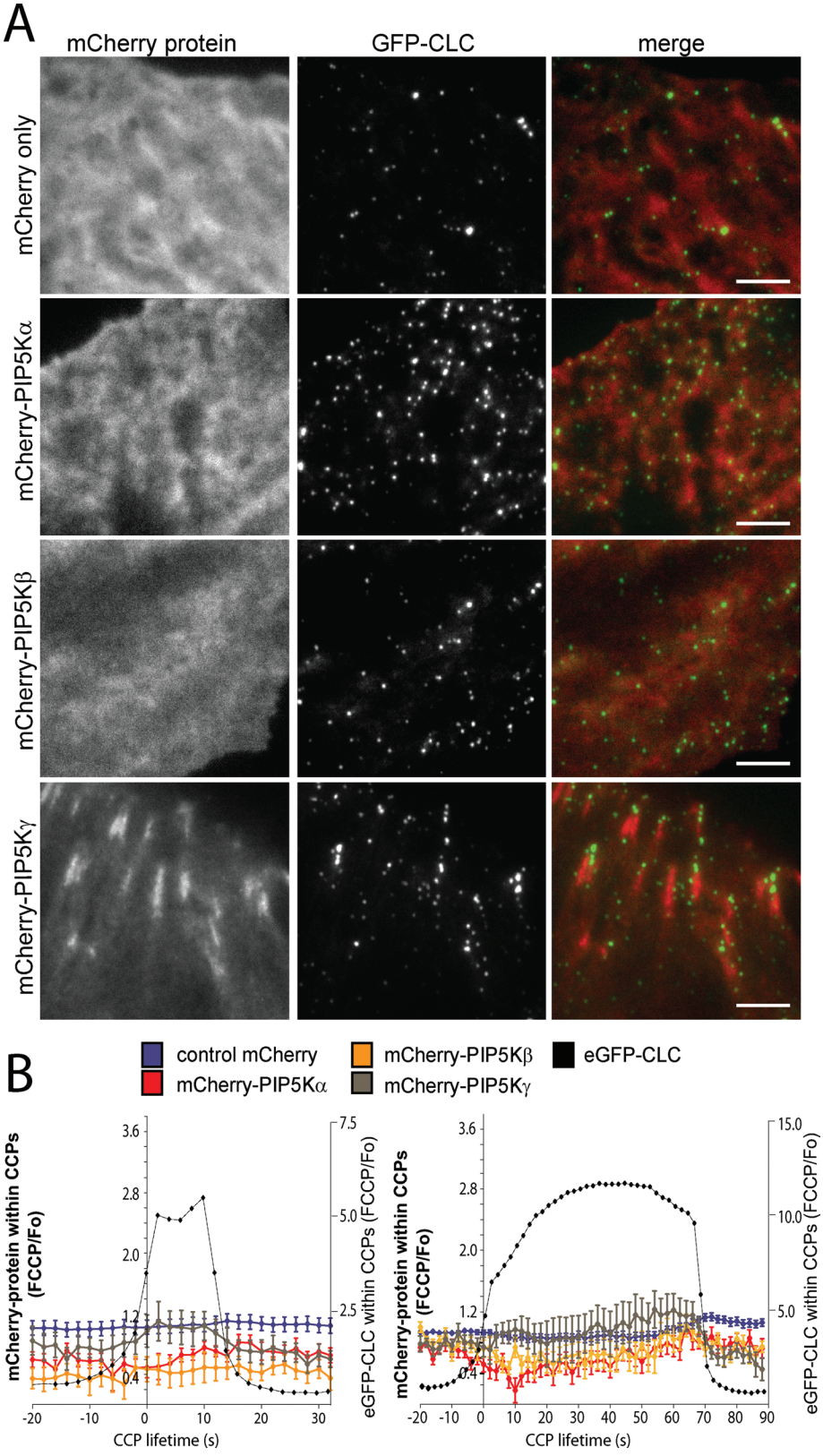

FIGURE 1: PIP5K isoforms cannot be detected in CCPs. BSC-1 cells stably expressing eGFP-CLC were transfected with cDNA encoding mCherry-PIP5Kα, mCherry-PIP5Kβ, mCherry-PIP5Kγ, or mCherry alone. Their dynamic localization to CCPs was detected by time-lapse TIRF microscopy. (A) Shown are representative single-frame fluorescence micrographs (also see Supplemental Movies 1–4). Scale bar, 5 μm. (B) Shown is the mean fluorescence intensity corresponding to mCherry-PIP5Kα, -PIP5Kβ, or -PIP5Kγ throughout CCP lifetimes within CCP tracks (alongside that of mCherry alone) grouped into 10–20 s (left panel) or 60–80 s (right panel) lifetime cohorts. Also shown is the mean fluorescence intensity of eGFP-CLC within these CCP tracks (note different scale). Error bars reflect cell-to-cell variation. The number of CCP trajectories (n) and cells (k) for each condition are control mCherry: n = 63,603, k = 50; mCherry-PIP5Kα: n = 74,685, k = 37; mCherry-PIP5Kβ: n = 62,130, k = 38; and mCherry-PIP5Kγ: n = 60,853, k = 33.

at higher levels of PIP5Kα overexpression (Figure 2B).

To understand how increased PIP_2 synthesis impacts CCV formation, we examined the effect of low levels of overexpression of PIP5Kα on CCP dynamics (i.e., under conditions that minimally perturb CME shown in Figure 2B). Under these conditions (at 15 ng/ml tet), overexpression of mCherry-PIP5Kα, but not KD, resulted in an increase in CCP initiation (Figure 2C), without affecting the lifetime of abortive (Figure 2D) or productive (Figure 2E) CCPs. Furthermore, there was no effect of PIP5K overexpression on the proportion of productive CCPs (Figure 2F). Similar results were obtained when we transiently transfected BSC-1 cells stably expressing eGFP-CLC with cDNA encoding mCherry-tagged PIP5K α, β, or γ and measured CCP dynamics in cells expressing the lowest detectable levels of mCherry-PIP5K (Supplemental Figure 1).

Although small, the increase in CCP initiation density observed upon PIP5K overexpression in the absence of other changes in CCP dynamics would be expected to increase (rather than decrease) rates of Tfn uptake. These findings suggest that an increase in PIP_2 levels may uncouple CCP formation and maturation from regulation by cargo (such as Tfn receptor [TfR]). As such, increased PIP_2 levels may result in formation of CCPs that have fewer cargo molecules, resulting in decreased internalization of cargo proteins, such as Tfn.

Increased PIP_2 synthesis regulates CCP size

We have previously shown that CCP size is, in part, regulated by incorporation of specific adaptors (Liu *et al.*, 2010; Mettlen *et al.*, 2010). We measured the intensity of clathrin in short- and longer-lived cohorts of diffraction-limited CCPs over their lifetime in control cells and cells overexpressing controlled, low levels of PIP5Kα WT (Figure 3) or transiently transfected with cDNAs encoding PIPK5α, β, or γ (Supplemental Figure 2, A–D). With regard to clathrin fluorescence, CCPs exhibit an initial growth phase, followed by a plateau phase during which they reach maximum clathrin intensity, before undergoing a

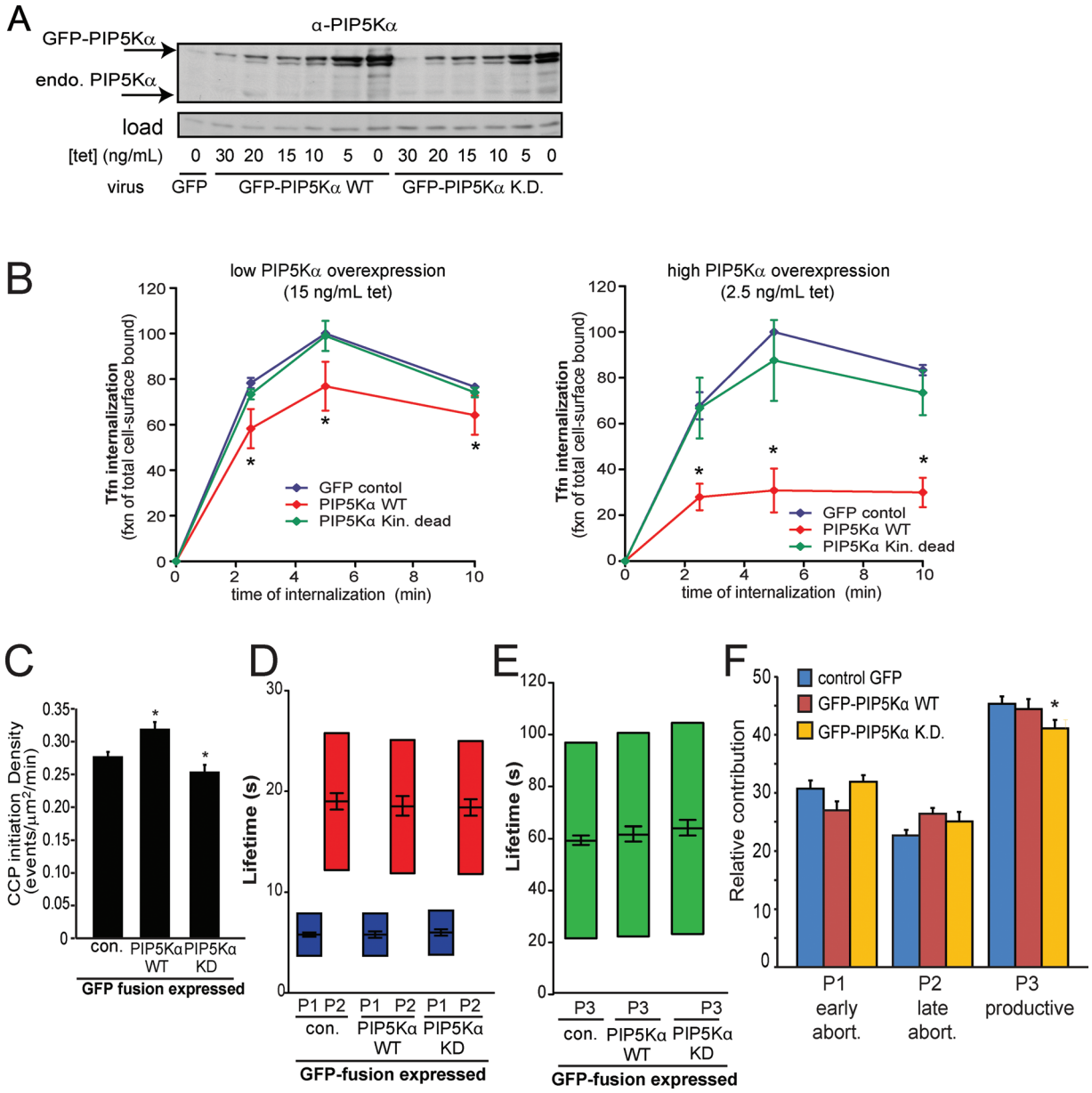

FIGURE 2: Controlled PIP5Kα overexpression reduces Tfn internalization yet increases CCP initiation. BSC-1 cells stably expressing mCherry-CLC were infected with adenoviruses encoding tet-regulated WT or KD eGFP-PIP5Kα or eGFP alone, and were cultured in the presence of various concentrations of tet. (A) Shown are representative immunoblots with anti-PIP5Kα. (B) Tfn uptake was determined in BSC-1 cells expressing either WT or KD PIP5Kα or GFP alone (control) at either 15 ng/ml (low overexpression) or 2.5 ng/ml (high overexpression) tet. Shown are the means of at least three independent experiments. (C–F) The results of TIRF microscopy imaging and CCP lifetime decomposition in cells infected with adenoviruses as indicated at 15 ng/ml tet are shown: (C) CCP initiation rate, lifetimes of abortive (D) and productive (E) CCP subpopulations, and (F) relative contributions of CCP subpopulations. Error bars, cell-to-cell variation; the length of the lifetime bars in (D) and (E) denotes the t_{50} spread of the distribution. The number of CCP trajectories (n) and cells (k) for each condition are control eGFP: n = 185,683, k = 73; eGFP-PIP5Kα WT: n = 177,504, k = 57; and eGFP-PI5K1α KD: n = 87,597, k = 38. (B and C) *$p < 0.05$. (D–F) *$p < 10^{-8}$.

rapid decay as the CCP moves away from the PM, resulting from scission and/or clathrin uncoating (Figure 3A; Loerke *et al.*, 2011). Adenovirus-mediated controlled expression of PIP5Kα increased the maximum eGFP-CLC fluorescence within CCPs of all lifetime cohorts (Figure 3B), as a result of increasing the initial rate of clathrin assembly, without changing the duration of the growth phase (Figure 3A). Overexpression by cDNA transfection of each of the three active PIP5K isoforms, but not the KD mutant of PIP5Kα, resulted in similar, yet more pronounced effects on these parameters (Supplemental Figure 2, A–D). That increases in clathrin fluorescence within CCP tracks do indeed reflect increased CCP size has previously been confirmed by electron microscopy (Mettlen *et al.*, 2010). Hence increased PIP_2 synthesis within the bulk PM enhances early stages of CCP initiation and growth.

PIP_2 synthesis is required for CCP assembly and stabilization

To determine the effect of reduced PIP_2 synthesis on CCP dynamics and size, we reduced the expression levels of each PIP5K isoform by

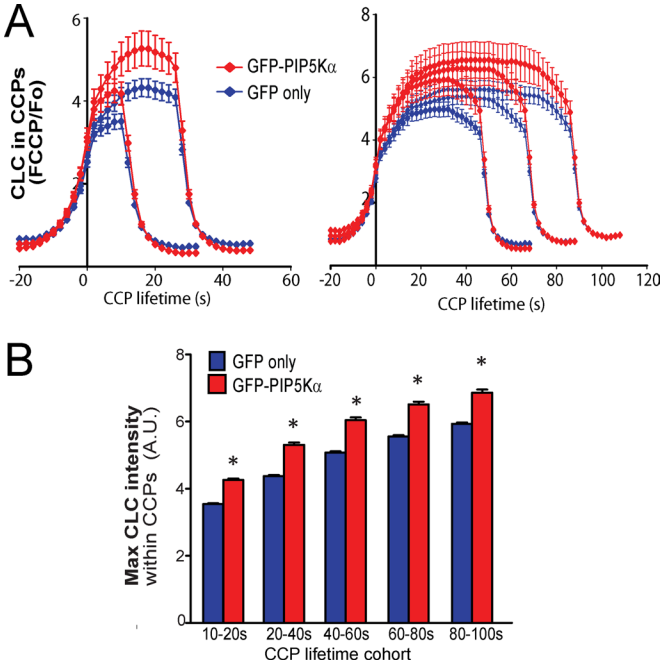

FIGURE 3: PIP5Kα overexpression increases CCP size. BSC-1 cells stably expressing mCherry-CLC were infected with adenoviruses encoding tet-regulated WT eGFP-PIP5Kα or eGFP alone, and were cultured in the presence of 15 ng/ml tet (low PIP5Kα overexpression). Shown is the mean mCherry-CLC (clathrin) fluorescence intensity throughout CCP lifetimes (A) or maximal mCherry-CLC in each CCP track (B), grouped into lifetime cohorts. Error bars reflect cell-to-cell variation. The number of CCP trajectories (n) and cells (k) for each condition are control eGFP: n = 185,683, k = 73; eGFP-PIP5Kα WT: n = 177,504, k = 57; and eGFP-PI5K1α KD: n = 87,597, k = 38. (B and C) *p < 0.05. (C, E, and F) *p < 10^{-8}.

siRNA. Although PIP5Kβ and γ could not be detected at the protein level, we were able to detect knockdown of their respective mRNAs (Supplemental Figure 3, B and C). These two treatments, however, also resulted in a robust, presumably compensatory, reduction of Sjn2 levels (Supplemental Figure 3F), and it was therefore not possible to unambiguously measure their role in CME. In contrast, PIP5Kα was readily detected by immunoblot, and siRNA knockdown resulted in a 60.0 ± 5.2% (n = 3) reduction in its mRNA and a corresponding reduction in protein levels (Figure 4A and inset, respectively) without affecting the levels of any other lipid kinase or phosphatase examined (Supplemental Figure 3, A–F).

Knockdown of PIP5Kα did not affect the lifetime of abortive or productive CCPs (Figure 4, C and D) but reduced CCP initiation density (Figure 4B) and decreased the proportion of productive CCPs (Figure 4E). The rate of Tfn internalization was not significantly affected (Supplemental Figure 3G). Knockdown of PIP5Kα also decreased the maximum fluorescence intensity of eGFP-CLC in CCPs (Figure 4F) by decreasing the initial rate of CCP assembly without altering the duration of the eGFP-CLC growth phase (Supplemental Figure 2E). The effect of simultaneous knockdown of all three PIP5K isoforms was indistinguishable from knockdown of PIP5Kα alone (unpublished data), and thus we conclude that PIP5Kα is the major isoform regulating CME in BSC-1 cells. Together with the results of PIP5K overexpression, these findings suggest that PIP_2 synthesis is limiting for the initial rate and extent of clathrin assembly at steady state, and, when PIP5Kα levels are reduced, PIP_2 synthesis also becomes limiting for CCP maturation efficiency.

5′-inositol phosphatases are detected in CCPs

In contrast to the PIP5Ks, we could detect the mCherry-tagged 5′-inositol phosphatases Sjn1 (170 kDa isoform, henceforth termed Sjn1–170), OCRLa, and Sjn2 at CCPs by dual-channel, time-lapse TIRF microscopy; however, there was considerable heterogeneity in the extent and the dynamic behavior of their recruitment (see Supplemental Movies 5–7 and representative single frames in Figure 5A). To better characterize the nature of their CCP association, we developed algorithms that can identify the presence of fluorescently tagged proteins within tracks of individual CCPs. mCherry-OCRLa and -Sjn2 were detected in only a small subset of CCPs (26.6 ± 3.2% and 25.6 ± 2.1%, respectively; Figure 5B). Moreover, both exhibited highly heterogeneous temporal recruitment to these pits: OCRLa was detected either throughout or only near the end of the lifetime of CCPs, and Sjn2 recruitment peaked either before significant clathrin accumulation or near the end of the lifetime of CCPs (see Supplemental Movies 5 and 6 and Supplemental Figures 4 and 5 for time-lapse montages of individual representative CCPs). mCherry-Sjn2 puncta not corresponding to CCPs, as well as Sjn2-labeled dynamic motile tubules, were also observed (Supplemental Movie 6). The nature and function of the Sjn2-labeled tubules remain to be determined. Given that mCherry-OCRLa and -Sjn2 exhibited recruitment to only a small subset of CCPs for only a small portion of their total lifetime, these phosphatases were rarely detected in CCPs at any single time (Figure 5A).

In contrast, mCherry-Sjn1–170 could be readily observed to colocalize with CCPs when examining single fluorescence micrographs (Figure 5A) or time-lapse movies (Supplemental Movie 7); correspondingly, Sjn1–170 was detected in a larger proportion (45.8 ± 3.2%) of CCPs (Figure 5B). Note that this is likely an underestimate of the percentage of CCPs containing Sjn1–170, given the stringency of our automatic detection of Sjn1–170 within CCPs (see *Materials and Methods*). Also in contrast to OCRLa and Sjn2, the dynamics of Sjn1–170 association with CCPs was largely homogenous (see Supplemental Figure 6 for time-lapse montages of individual representative CCPs). Averaging of mCherry-Sjn1–170 fluorescence intensity within CCP tracks for both short-lived (Figure 5C, top) and longer-lived (Figure 5C, bottom) CCPs (n > 30,000) revealed a temporal recruitment profile similar to that of eGFP-CLC. The presence of 5′-inositol phosphatases in CCPs suggests that localized PIP_2 turnover occurs during CCV formation and, of those examined, Sjn1–170 appears to be the principal 5′-inositol phosphatase specifically recruited to CCPs in BSC-1 cells.

Activity-dependent and -independent effects of 5′-inositol phosphatase overexpression on CCP assembly and maturation

To better understand the role of Sjn1–170 within CCPs, we examined the effect of its controlled overexpression on Tfn uptake and CCP dynamics. Using the same tet-regulated adenovirus strategy as for PIP5Kα, we expressed eGFP-Sjn1–170 (WT or 5′-inositol phosphatase-dead [PD]) in BSC-1 cells (Figure 6A). Overexpression of Sjn1–170 WT at low levels did not measurably impact Tfn uptake (Figure 6B). At higher levels of overexpression, however, Tfn uptake was reduced, but this effect was also observed upon overexpression of Sjn1–170 PD (Figure 6B). This reduction in Tfn uptake could reflect activity-independent sequestration of other endocytic proteins and/or the displacement of phosphatase active, endogenous Sjn1 from CCPs.

To define which stage(s) of CCP assembly and maturation might be affected by Sjn1, we examined CCP dynamics in cells overexpressing WT and PD mCherry-Sjn1–170 under conditions that minimally perturb CME. Low levels of Sjn1 WT overexpression did not

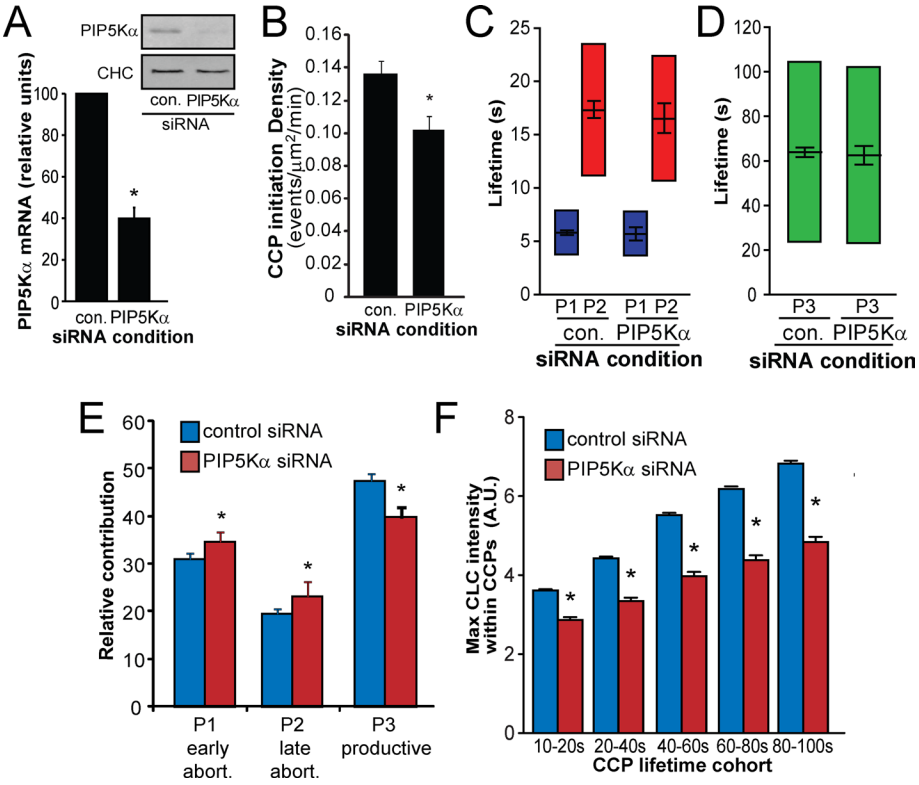

FIGURE 4: siRNA knockdown of PIP5Kα reduces CCP maturation efficiency and CCP size. BSC-1 cells stably expressing eGFP-CLC were treated with PIP5Kα-specific or nontargeting (control) siRNA. (A) Shown are the means of at least three independent experiments for detection of PIP5Kα mRNA levels and a representative immunoblot with PIP5Kα-specific or CHC-specific (loading control) antibodies. The results of TIRF microscopy imaging and CCP lifetime decomposition in cells treated with siRNAs as indicated are shown: (B) CCP initiation rate lifetimes of (C) abortive and (D) productive CCP subpopulations and (E) relative contributions of CCP subpopulations. The length of the lifetime bars in (C) and (D) denotes the t_{50} spread of the distribution. (F) Mean maximal eGFP-CLC intensity within CCP tracks grouped into lifetime cohorts was determined in cells treated as indicated. Error bars reflect cell-to-cell variation. The number of CCP trajectories (n) and cells (k) for each condition are control siRNA: n = 102,059, k = 81; and PIP5Kα siRNA: n = 30,828, k = 34. (A, B, and F) *p < 0.05. (C–E) *p < 10^{-8}.

impact CCP initiation (Figure 6C) or alter the lifetime of productive CCPs (Figure 6E). Instead, Sjn1–170 WT overexpression reduced the lifetime of abortive CCPs (Figure 6D) and the proportion of productive CCPs (Figure 6F). These effects, which were more pronounced in transiently transfected cells that presumably express higher levels of mCherry-Sjn1–170 WT (Supplemental Figure 7), were not observed in cells overexpressing Sjn1–170-PD (Figure 6, D–F, Supplemental Figure 7). Thus, the effects of Sjn1 on early stages of CCP stabilization and maturation were dependent on phosphatase activity and hence changes in the rates or extents of PIP_2 turnover. Finally, unlike PIP5K overexpression, Sjn1–170 overexpression did not alter either the rate of incorporation of eGFP-CLC or CCP size (unpublished data).

Overexpression of Sjn1–170 PD, even at controlled levels, resulted in dominant-negative effects that were distinct from those resulting from Sjn1–170 WT overexpression. These effects included a slight reduction in the initiation density of CCPs (Figure 6C) and an increased lifetime of productive CCPs (Figure 6E, Supplemental Figure 7). Sjn1–170 contains a proline-rich domain, an NPF sequence that binds Eps15, as well as binding sites for AP-2 and clathrin (Perera *et al.*, 2006); therefore these effects likely reflect displacement of endogenous EAPs, including active Sjn1, from their CCP binding partners. That these effects differ from the effects of overexpression of phosphatase-active Sjn1 suggests that localized PIP_2-phosphatase activity might control the dynamics of protein interactions during CCP assembly and maturation. We also overexpressed mCherry-OCRLa or –Sjn2 constructs but found no differences in the effects of WT versus their PD mutants on CCP dynamics (unpublished data), making the interpretation of a role for the activities of these lipid phosphatases in CCV formation difficult. Together these findings suggest multiple distinct roles for PIP_2 degradation by Sjn1 during CCV formation.

To further probe whether the phosphatase-dependent effects of Sjn1–170 overexpression on CME and CCV formation were indeed due to its localization to CCPs, we transfected BSC-1 cells stably expressing eGFP-CLC with mCherry-Sjn1 145 (145 kDa isoform). This shorter isoform of Sjn1 lacks the NPF sequence and the binding motifs for AP-2 and clathrin and is recruited less efficiently to CCPs in COS cells (Perera *et al.*, 2006). Indeed mCherry-Sjn1–145 is observed to localize to CCPs far less efficiently than Sjn1–170 in BSC-1 cells (Supplemental Figure 8A, compare to Figure 5A). The effects of overexpression of Sjn1–145 WT on CCP lifetimes (Supplemental Figure 8, B and C) and maturation efficiency (Supplemental Figure 8D) were much smaller than those of Sjn1–170 WT and were not dependent on phosphatase activity as similar effects were seen upon overexpression of mCherry-Sjn1–145 PD (Supplemental Figure 8, B–D). These results suggest that any effects of overexpression of mCherry-Sjn1–145 were likely due to sequestration of other CCP components and not the result of localized PIP_2 hydrolysis within CCPs. Hence the phosphatase-dependent effects of Sjn1–170 on CCP dynamics were indeed likely due to its localization to CCPs.

siRNA knockdown of Sjn1 affects early and late stages of CCP maturation

To complement the findings obtained from overexpression studies, we also examined the effect of siRNA knockdown of Sjn1, which reduced its mRNA levels by 53.8 ± 6.7% (n = 7) (Figure 7A), and did not affect expression of other lipid kinases and phosphatases examined (Supplemental Figure 3). Sjn1 knockdown had no effect on CCP initiation (Figure 7B), consistent with the lack of effect of Sjn1 overexpression on this parameter. Knockdown of Sjn1 resulted in an increase in the proportion of productive CCPs (Figure 7E) and increased the lifetime of abortive CCPs (Figure 7C), producing the expected opposite effect of Sjn1–170 WT overexpression on these parameters. These findings suggest that the stability of nascent CCPs is controlled by localized, Sjn1-dependent PIP_2 turnover. Knockdown of Sjn1 also resulted in a longer lifetime of productive CCPs (Figure 7D), consistent with the effect of overexpression of Sjn1–170 PD (Figure 3F). Hence dephosphorylation of PIP_2 by Sjn1 also contributes to late stages of CCP maturation/uncoating. Knockdown of Sjn1 did not impact the size of CCPs (Figure 7F), consistent

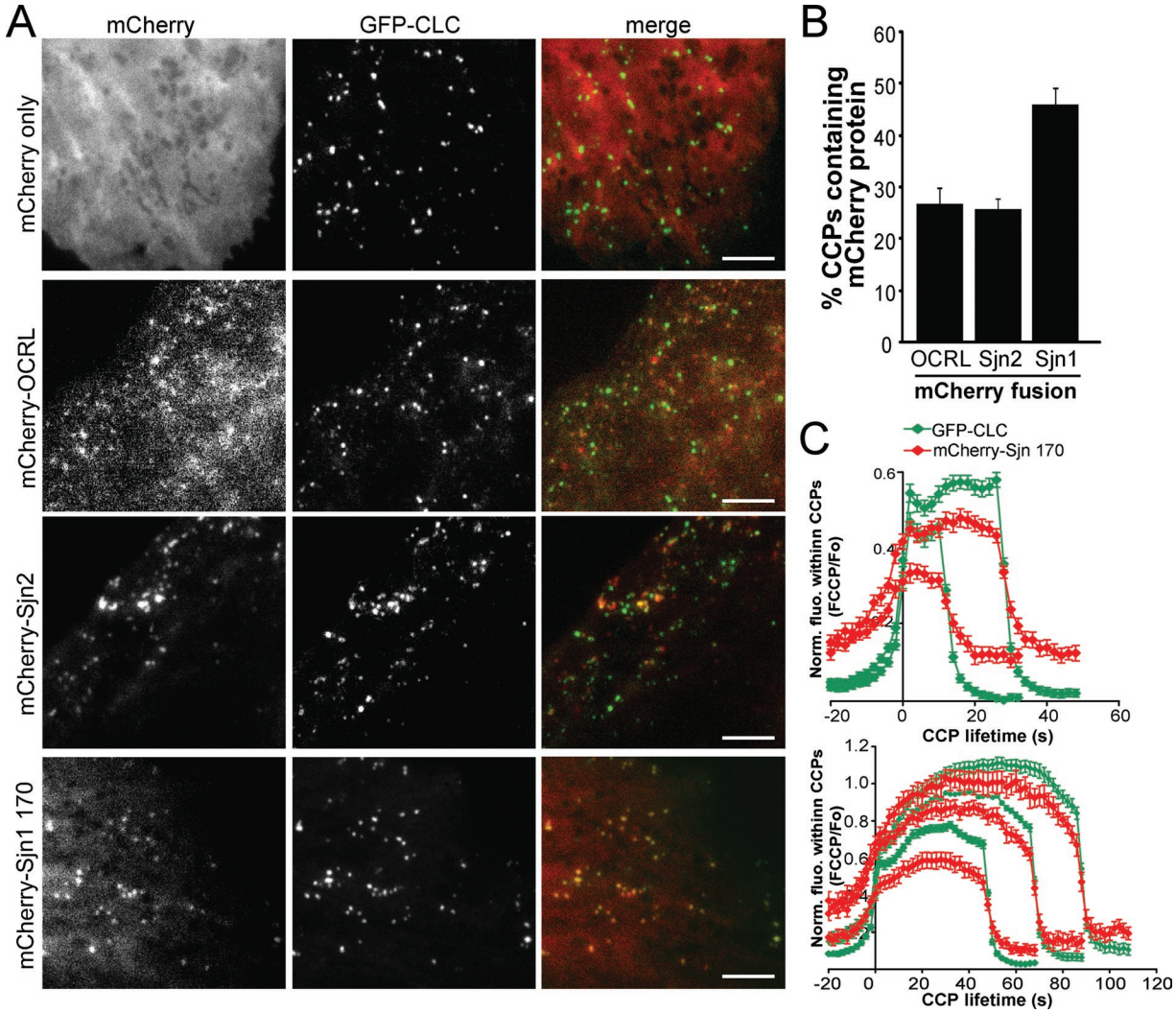

FIGURE 5: Sjn1 is the major 5′-inositol phosphatase within CCPs. BSC-1 cells stably expressing eGFP-CLC were transfected with cDNA encoding mCherry-Sjn1, mCherry-OCRL, mCherry-Sjn2, or mCherry alone. (A) Representative single-frame fluorescence micrographs acquired by TIRF microscopy are shown (also see Supplemental Movies 5–7). Scale bar, 5 μm. (B) CCP tracks with detectable mCherry-tagged phosphatases were computationally identified as described in *Materials and Methods*. Shown is the mean percentage of CCPs positive for each mCherry-tagged phosphatase. (C) Shown is the mean normalized fluorescence corresponding to eGFP-CLC or mCherry-Sjn1 in distinct CCP lifetime cohorts. Error bars represent cell-to-cell variation. The number of CCP trajectories (n) and cells (k) for each condition are control mCherry: n = 209,738, k = 78; mCherry-Sjn1 170: n = 80,709, k = 45; mCherry-OCRLa: n = 137,307, k = 29; mCherry-Sjn2: n = 73,871, k = 31.

with the lack of effect of Sjn1 overexpression on this parameter. Furthermore, knockdown of Sjn1 did not measurably alter the rate of Tfn uptake (Supplemental Figure 3H), consistent with these conditions representing a subtle perturbation of PIP_2 dynamics and/or the fact that Sjn1 exhibits both positive (productive CCP lifetimes) and negative (maturation efficiency) regulation of CCV formation.

Collectively these results suggest that the assembly and maturation efficiency of nascent CCPs are controlled in part by the opposing actions of PIP_2 synthesis and turnover. Moreover, there appears to be a temporal hierarchy in that initial rates of clathrin assembly are selectively dependent on the activity of PIP5Kα, whereas the turnover of nascent CCPs appears to be selectively dependent on Sjn1 activity, which also selectively contributes to the late stages of productive CCP maturation.

DISCUSSION

Much has been learned in recent years about the function of EAPs in CCV formation, but less is known about the role of specific phospholipids in this process. Here, we have used overexpression and siRNA-mediated knockdown of PIP5K and Sjn1 to show that PIP_2 synthesis and turnover contribute to multiple, yet only partly overlapping stages of CCV formation. Moreover, we find that PIP_2 synthesis and turnover are spatially segregated events as we were unable to detect colocalization of any of the three PIP5K isoforms within CCPs at any point during their lifetime, whereas all three 5′-inositol phosphatases we studied (OCRLa, Sjn2, and Sjn1) associated dynamically with at least a subset of CCPs. Thus, as previously suggested for the synapse (Wenk *et al.*, 2001), bulk PIP_2 levels appear to regulate CCP assembly, whereas localized turnover of PIP_2 controls multiple stages in CCV formation.

Knockout of PIP5Kγ, the major PIP5K isoform in neurons, inhibits early stages of clathrin-mediated recycling of synaptic vesicles (SVs) (Wenk *et al.*, 2001). Knockout of Sjn1 in mice (Cremona *et al.*, 1999) or of the only Sjn homologue in *Caenorhabditis elegans* (Harris *et al.*, 2000) similarly inhibits clathrin-mediated recycling of SVs and leads to the accumulation of multiple distinct intermediates in the

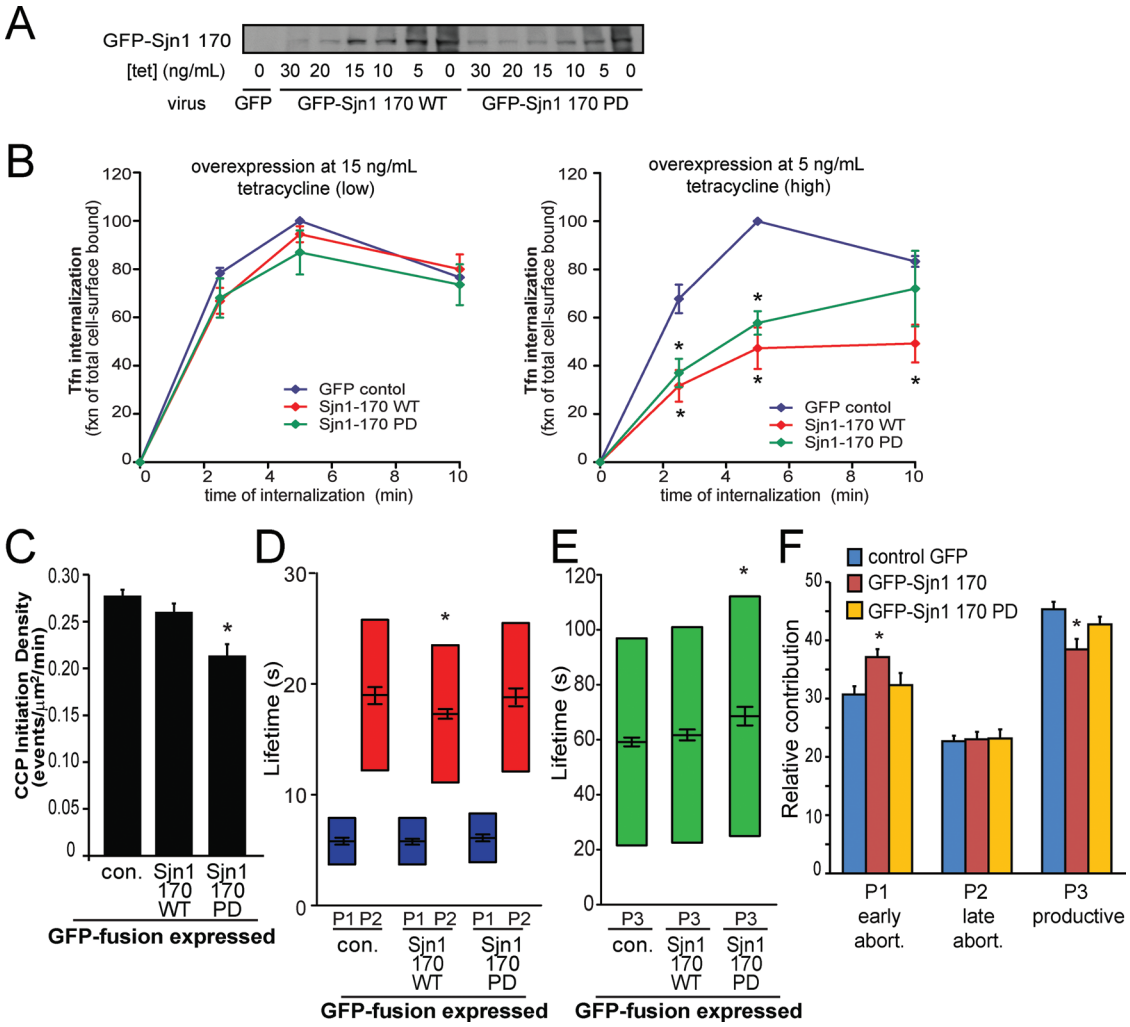

FIGURE 6: Controlled overexpression of Sjn1–170 impacts CCP stabilization, abortive turnover, and maturation. BSC-1 cells stably expressing mCherry-CLC were infected with adenoviruses encoding tet-regulated WT or PD eGFP-Sjn1 or eGFP alone and cultured in the presence of various concentrations of tet. (A) Shown is a representative immunoblot with anti-GFP antibodies to detect GFP-Sjn1 expression. (B) Tfn uptake was determined in BSC-1 cells expressing either WT or PD Sjn1–170 or GFP alone (control) at either 15 ng/ml (low overexpression) or 5 ng/ml (high overexpression) tet. Shown are the means of at least three independent experiments. (C–F) The results of TIRF microscopy imaging and CCP lifetime decomposition in cells infected with adenoviruses at 15 ng/ml tet as indicated are shown: (C) CCP initiation rate, lifetimes of (D) abortive and (E) productive CCP subpopulations, and (F) relative contributions of CCP subpopulations. Error bars reflect cell-to-cell variation; the length of the lifetime bars in (D) and (E) denotes the t_{50} spread of the distribution. The number of CCP trajectories (n) and cells (k) for each condition are control GFP: n = 185,683, k = 73; eGFP-Sjn1 170 WT: n = 85,212, k = 34; eGFP-Sjn1 170 PD: n = 44,651, k = 26. (B and C) *$p < 0.05$. (D–F) *$p < 10^{-8}$.

SV recycling pathways. In non-neuronal cells, CME is potently inhibited by acute recruitment of an overexpressed 5′-inositol phosphatase to the bulk PM (Zoncu *et al.*, 2007; Abe *et al.*, 2008). By controlling levels of overexpression of Sjn1–170 using a tet-regulated adenoviral expression system, we also observe inhibition of CME at high levels of expression, but not at lower levels. As Sjn1 is targeted to CCPs, this observation suggests that the spatial and temporal regulation of PIP_2 turnover can buffer the effects of moderate levels of overexpression. We used these mildly perturbing conditions to probe the role of PIP_2 turnover in CCP maturation.

At similarly low levels of overexpression of active, but not KD, PIP5Kα, we observed a small but significant decrease in the rate of Tfn endocytosis, which was more pronounced at higher levels of overexpression. These results differ from a previous report showing that overexpression of PIP5Kα in NR6 cells (Barbieri *et al.*, 2001) or β in CV-1 cells (Padron *et al.*, 2003) increases Tfn or EGF internalization, respectively. These differences may reflect the different experimental conditions and assays used. For example, Stahl and colleagues measured EGF uptake at 100 ng/ml (Barbieri *et al.*, 2001), conditions under which the EGF receptor was subsequently shown to internalize primarily via clathrin-independent mechanisms (Sigismund *et al.*, 2008). In addition, we have recently shown differential lipid dependence for EGF versus Tfn uptake via CME (Antonescu *et al.*, 2010). We also note that the previous study by Roth and colleagues did not measure Tfn internalization relative to surface TfR (Padron *et al.*, 2003). As the surface expression of TfR would increase under conditions that inhibit endocytosis, the absolute extent of Tfn accumulation under these conditions may not reflect the rate of Tfn internalization. Both the present (Figure 3, Supplemental Figure 2) and previous studies (Padron *et al.*, 2003),

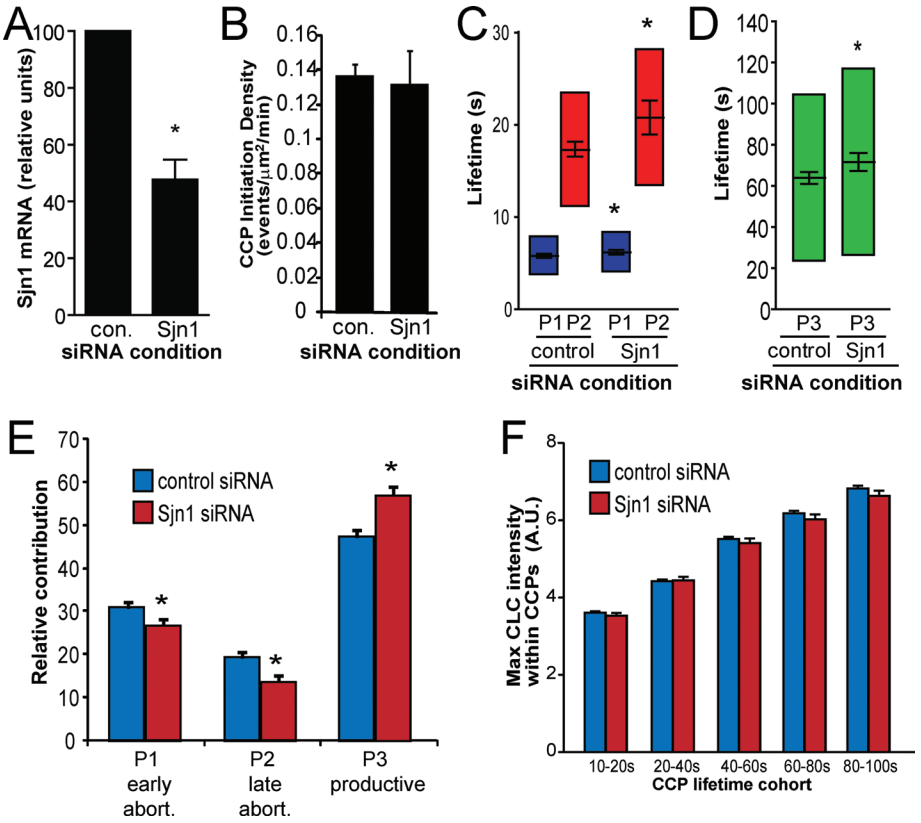

FIGURE 7: siRNA knockdown of Sjn1 enhances CCP maturation efficiency, delays the turnover of abortive CCPs, and increases the lifetime of productive CCPs. BSC-1 cells stably expressing eGFP-CLC were treated with either Sjn1-specific or nontargeting siRNA. (A) Shown are the means of at least five independent experiments for detection of Sjn1 mRNA levels. The results of TIRF microscopy imaging and CCP lifetime decomposition in cells treated with siRNAs as indicated are shown: (B) CCP initiation rate, lifetimes of (C) abortive and (D) productive CCP subpopulations, and (E) relative contributions of CCP subpopulations. (F) Mean maximal eGFP-CLC (clathrin) fluorescence intensity within CCP tracks grouped into lifetime cohorts was determined in cells treated as indicated. Error bars reflect cell-to-cell variation; the length of the lifetime bars in (C) and (D) denotes the t_{50} spread of the distribution. The number of CCP trajectories (n) and cells (k) for each condition are control siRNA: n = 10,259, k = 81; and Sjn1 siRNA: n = 42,649, k = 33. (A) *$p < 0.05$. (C–E) *$p < 10^{-8}$.

however, reported an increase in CCP density upon PIP5K overexpression. Together these studies have defined a critical role for PIP_2 in CME and suggest that examination of CCP dynamics in addition to cargo internalization is required to understand the function of endocytic factors in CME.

By quantitative live-cell imaging of CCPs we have previously identified discrete stages of CCV formation (Figure 8) (Loerke *et al.*, 2009; Mettlen *et al.*, 2009, 2010; Antonescu *et al.*, 2010; Loerke *et al.*, 2011). CCP initiation occurs as a result of a rapid burst of clathrin recruitment (~2 s) and is followed by a period (~20–30 s) of CCP assembly/growth (Loerke *et al.*, 2011). A large fraction of CCPs rapidly disassemble (so-called abortive CCPs; Ehrlich *et al.*, 2004; Loerke *et al.*, 2009), which led us to propose that stabilization of nascent CCPs corresponds to crossing an endocytosis "checkpoint" that monitors the fidelity of CCP assembly (Loerke *et al.*, 2009). Although still poorly defined, factors that determine progression beyond this checkpoint, which include the rate and nature of coat assembly, cargo loading, and curvature generation, affect the efficiency of CCP maturation and hence the ratio of abortive versus productive CCPs (Loerke *et al.*, 2009, 2011; Mettlen *et al.*, 2009, 2010; Lui *et al.*, 2010). Stabilized CCPs then proceed through a maturation phase of variable length during which the total amount of clathrin is largely constant (Mettlen *et al.*, 2010; Loerke *et al.*, 2011). Finally, CCPs undergo inward movement, followed by rapid scission and uncoating (Merrifield *et al.*, 2005; Saffarian and Kirchhausen, 2008; Loerke *et al.*, 2011). Using these quantitative live-cell assays to independently measure CCP initiation rates, intensity changes (i.e., growth), maturation efficiency, and the lifetimes of both abortive and productive CCPs, we detect multiple, differentiated roles of PIP_2 synthesis and turnover during CCV formation.

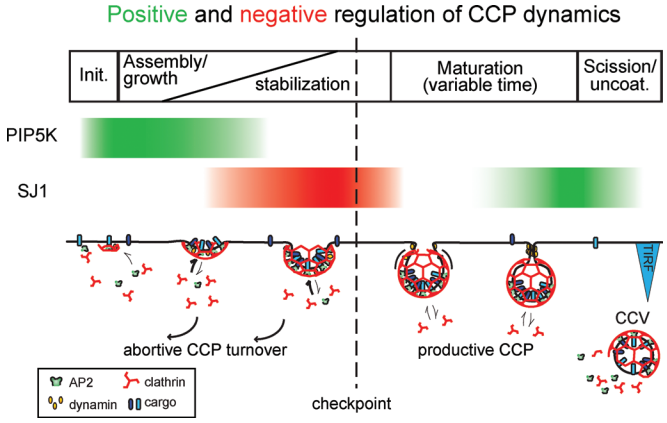

FIGURE 8: Diagram depicting temporal regulation of CCP formation by PIP5K and Sjn1. Stages of CCP formation (initiation, assembly/growth, which leads to stabilization, maturation, and scission/uncoating). Dotted line indicates the proposed endocytic checkpoint that gates progression toward CCV formation. Positive (green) and negative (red) regulation by PI5K and Sjn1 at each stage is also shown. See *Discussion* for details.

Regulation of CCP initiation and growth by PIP_2

PIP_2 synthesis by PIP5K, but not its turnover by Sjn1, regulates CCP initiation (Figure 8). This difference may be a consequence of the different localization of these two enzymes relative to CCPs. We infer that global PIP_2 synthesis is the major determinant of PIP_2 availability for CCP initiation. CCP initiation must precede the significant localized accumulation of 5′-inositol phosphatases such as Sjn1 as they are recruited through interactions with coat proteins. Because AP-2 is also limiting for CCP initiation (Loerke *et al.*, 2009), the requirement for bulk PIP_2 at this earliest stage may reflect the need for a PIP_2-stabilized conformational change in AP-2 upon cargo binding (Jackson *et al.*, 2010). Alternatively, or in addition, PIP_2 may be required for the membrane targeting of the FCHo/intersectin/Eps15 protein complex, recently shown to be critical in CCP nucleation (Henne *et al.*, 2010).

Levels of PIP5Kα activity, but not those of Sjn1, influence the rate and extent of CCP growth (Figure 8). We have previously determined that the size of CCPs is regulated by their content of adaptor-bound

cargo molecules, such as TfR/AP-2 (Liu *et al.*, 2010) and low-density lipoprotein receptor bound to Dab2/ARH (Mettlen *et al.*, 2010). Here we show that PIP5K-mediated PIP_2 synthesis works in concert with cargo/adaptor complexes to regulate the rate of incorporation of clathrin during the initiation and growth phases of CCPs, which in turn determines their size. Clathrin assembly occurs at the boundary of CCPs and bulk PM; thus, it is under the influence of globally synthesized PIP_2 and not of CCP-localized lipid phosphatases. Indeed, labeling of freeze-fractured membranes with a gold-conjugated PH-domain probe revealed that PIP_2 is depleted from the center of a coated pit relative to its periphery (Fujita *et al.*, 2009). Interestingly, although neither knockdown nor overexpression of Sjn1 affected the rate of CCP assembly or CCP size, a recent study found that the phosphatase SHIP2 negatively regulates the rate of CCP growth (Nakatsu *et al.*, 2010). Thus, during early stages of CCP assembly, PIP_2 synthesis by PIP5Ks in the bulk PM may be negatively regulated and/or counterbalanced locally by SHIP2.

Regulation of CCP stabilization by PIP_2

The contributions of PIP_2 to the rate of incorporation of clathrin into the growing coat versus its role in CCP stabilization appear to be at least partly independent. PIP5K overexpression increased CCP size without affecting the rate of turnover of abortive CCPs, whereas increasing or decreasing Sjn1 levels decreased or increased the rate of turnover of abortive CCPs, respectively, without affecting CCP size. We have recently shown that the initial rate of clathrin incorporation is similar between CCPs of different lifetimes; whereas short-lived (i.e., unstable), abortive CCPs exhibit a reduced initial rate of AP-2 incorporation compared with longer-lived (i.e., stabilized), productive CCPs (Loerke *et al.*, 2011). Together these data argue that stabilization of CCPs during the assembly/growth stage does not depend on clathrin self-assembly but instead depends on the rate of incorporation of AP-2 and PIP_2, which together can serve as ligands for the web of low-affinity protein interactions that occur early in CCP formation (Schmid and McMahon, 2007). Our data further suggest that the local hydrolysis of PIP_2 contributes to the destabilization and disassembly of abortive CCPs. Sjn1 is recruited to CCPs via interactions with the α-ear domain of AP-2 and the N-terminal domain of clathrin heavy chain (CHC; Praefcke *et al.*, 2004; Schmid and McMahon, 2007). Hence Sjn1 recruitment might be expected to occur predominantly within early-stage CCPs that are deficient in recruitment of other EAPs to the ear domains of AP-2 and to the N-terminal domain of CHC. Sjn1 may thus facilitate destabilization and turnover of nascent CCPs harboring defects in EAP recruitment, thereby freeing coat components for reassembly into new CCPs.

The inhibition of PIP_2 synthesis and turnover by siRNA knockdown of PIP5Kα and Sjn1, respectively, had reciprocal effects on CCP maturation efficiency: Knockdown of PIP5Kα reduced the proportion of productive CCPs, whereas knockdown of Sjn1 enhanced this parameter. Consistent with this finding, overexpression of Sjn1, but not PD Sjn1, resulted in a large decrease in the proportion of productive CCPs. In contrast, overexpression of PIP5K did not affect this parameter. The presence of 5′-inositol phosphatases such as Sjn1 within CCPs may explain this observation in that localized dephosphorylation could mitigate the PIP5K-dependent increases in bulk PIP_2 on CCP dynamics. Together these findings indicate that local concentrations of PIP_2 contribute to progression beyond the endocytosis checkpoint and stabilization of nascent CCPs.

Regulation of cargo loading by PIP_2

Interestingly, increased global PIP_2 production resulting from overexpression of PIP5Kα reduces the rate of Tfn internalization in BSC-1 cells. By quantifying the fluorescence intensity corresponding to TfR within CCPs in a manner similar to that done here for PIP5K (Figure 1) and Sjn1 (Figure 5), maximal cargo loading was shown to occur early (within ~5 s) in the lifetime of CCPs (Liu *et al.*, 2010), even though the AP-2 content continues to increase beyond this stage (~20–30 s). (Loerke *et al.*, 2011). This finding suggests that although AP-2 is initially recruited to the PM in part by binding cargo proteins, subsequent AP-2 recruitment into CCPs occurs predominantly by other interactions, such as that with PIP_2, contributing to stabilization of nascent CCPs. Together these studies suggest that increasing PIP_2 levels by overexpression of PIP5K increases the initiation of CCPs that contain few cargo molecules, as adaptor proteins are recruited to and become stabilized on the PM predominantly by PIP_2. This reduced dependence on cargo could, in turn, lead to internalization of CCPs that contain adaptor proteins that are relatively devoid of TfR, thus effectively abrogating the control of CCP maturation by their cargo content, which occurs under conditions of unperturbed PIP_2 synthesis (Loerke *et al.*, 2009; Mettlen *et al.*, 2010). As such, overproduction of PIP_2 may represent a bypass of the endocytic checkpoint that normally ensures that only CCPs effectively loaded with cargo become stabilized.

Conversely, silencing of PIP5Kα did not detectably reduce Tfn uptake while CCP initiation and stabilization were reduced, suggesting that under this condition of mild reduction of PIP_2 synthesis, the stabilization of nascent CCPs becomes more dependent on cargo proteins. In other words, the increase in abortive CCPs seen upon PIP5Kα knockdown likely reflects turnover of those CCPs containing the fewest cargo molecules and hence that are most susceptible to destabilization by reductions in global PIP_2 levels. The remaining, cargo-rich CCPs mature and internalize normally, resulting in only small changes in cargo internalization that are difficult to detect by measurement of Tfn uptake. Hence, due to the regulation of CCV formation by PIP_2, cargo internalization by CME may be inherently buffered against modest reductions in PIP_2 levels, such as following activation of PLCγ by growth factor stimulation. More robust reductions in PIP_2 levels lead to loss of AP-2 (Abe *et al.*, 2008) or clathrin (Malecz *et al.*, 2000; Zoncu *et al.*, 2007) from the PM, and completely abrogate cargo internalization.

Regulation of late stages of CCV formation by PIP_2

A maturation period of variable length follows progression beyond the checkpoint, ultimately culminating in CCV scission and uncoating (Figure 8). Perturbations of endocytic proteins that alter the lifetime of productive CCPs imply a role for these factors in CCP maturation, scission, and/or uncoating. We have previously shown that knockdown of epsin, Eps15, Hip1R, intersectin, and dynamin increases the lifetime of productive CCPs (Loerke *et al.*, 2009; Mettlen *et al.*, 2009), suggesting their requirement for late stages of CCV formation. Interestingly, the lifetime of productive CCPs was unaffected either by partial knockdown of PIP5Kα or overexpression of Sjn1. These results suggest that, after progression beyond the checkpoint, PIP_2 synthesis is no longer limiting for CCP maturation and CCV formation. Based on competitive binding of clathrin and EAPs to the β-ear of AP-2, it has been proposed that, during the process of accumulation of clathrin within CCPs, the interaction hub for EAP recruitment "switches" from the AP-2 ear to the clathrin N-terminal domain (Schmid *et al.*, 2006). During the assembly stage of CCP formation, AP-2 recruitment reaches its maximum whereas clathrin continues to accumulate before also reaching a plateau (Loerke *et al.*, 2011). Hence, after crossing a stability threshold during CCP assembly, there may no longer be a significant requirement for PIP_2 as a membrane ligand for recruitment of AP-2 and other EAPs.

In contrast to the effects of reducing PIP_2 availability by PIP5Kα knockdown or Sjn1 overexpression, knockdown of Sjn1 increased the lifetime of productive CCPs. This finding suggests that PIP_2 turnover within CCPs might be required during the late stages of CCV formation (Figure 8). Indeed, PIP_2 asymmetry at the neck of invaginated CCPs has been proposed to be a contributing force for membrane fission (Liu *et al.*, 2009), and a recent study showed that the phosphatase activity of Sjn1 facilitates scission of highly curved membrane tubules (Chang-Ileto *et al.*, 2011). Sjn1 knockout mice exhibit an increase in the number of CCVs, implying that these 5′-inositol phosphatases might also be required for clathrin uncoating following CCV formation (Cremona *et al.*, 1999; Kim *et al.*, 2002). Thus, the prolonged lifetime of CCPs upon Sjn1 knockdown may reflect events occurring after vesicle formation rather than during the maturation stage as uncoated CCVs could remain at the cell periphery within the TIRF field (Taylor *et al.*, 2011). Further studies are necessary to determine the role of lipid phosphatases in these late-stage events.

Although methods are not available to directly follow local PIP_2 production and turnover at CCPs, our results imply spatially and temporally distinct roles for the dynamic regulation of PIP_2 at different stages of CCV formation. At each stage, PIP_2 might function as a ligand, regulator, and/or structural component. Using similar methods, we have recently shown that phosphatidic acid regulates both early (CCP initiation) and late stages (lifetime of productive CCPs) of CCV formation without impacting CCV maturation efficiency (i.e., CCP stability) (Antonescu *et al.*, 2010). Thus, phosphatidic acid and PIP_2 have distinct contributions to CCV formation. Together these studies begin to reveal the complexity and unravel the spatiotemporal impact of lipid dynamics on CCV formation in mammalian cells.

MATERIALS AND METHODS

Cell culture and Tfn uptake

Epithelial BSC-1 monkey kidney cells stably expressing eGFP-CLC were provided by T. Kirchhausen (Harvard Medical School, Boston, MA). BSC-1 cells were grown in DMEM supplemented with 20 mM HEPES, 10 μg/ml streptomycin, 66 μg/ml penicillin, 10% (vol/vol) fetal calf serum (Hyclone, Logan, UT), supplemented with 0.5 mg/ml G418 (Invitrogen, Carlsbad, CA), under 5% CO_2 at 37°C.

CME of Tfn was analyzed as previously described by measuring the uptake of biotinylated Tfn as a function of time and expressed as a fraction of total initial cell surface Tfn binding (Antonescu *et al.*, 2010).

cDNAs, transfection, and adenovirus-mediated expression

All PIP5K isoform designations herein refer to the human nomenclature. cDNAs encoding full-length mouse PIP5Kα, β, and γ (661 amino acid isoform) were subcloned in-frame downstream of mCherry to create the respective N-terminal mCherry-PIP5K fusion proteins. cDNA encoding GFP-Sjn1 (170 kDa isoform) and GFP-Sjn2 (Sjn2B; Malecz *et al.*, 2000) were gifts from Pietro De Camili (Yale University, New Haven, CT) and Mark Symons (Feinstein Institute for Medical Research, Manhasset, NY), respectively, and were used to create mCherry-tagged versions of each phosphatase. cDNA encoding mCherry-OCRLa was a gift of Martin Lowe (University of Manchester, UK). cDNA encoding kinase-inactive PIP5Kα mutant (D268A; here termed KD) was made by site-directed mutagenesis, as described previously (Tolias *et al.*, 1998). cDNA encoding 5′-inositol phosphatase–inactive Sjn1 was made by site-directed mutagenesis (here termed PD) corresponding to R796A and R803A within Sjn2 (Rusk *et al.*, 2003).

To achieve efficient expression of eGFP-PIP5K1α, eGFP-Sjn1 (170), or eGFP alone (control) in BSC-1 cells, adenoviruses coding for these proteins under the control of a tet-regulated promoter were created. Following seeding, BSC-1 cells were infected with appropriate virus together with adenoviruses encoding a tet-repressible transcription activator. After overnight incubation in various amounts of tet (to allow various levels of eGFP-tagged protein expression; see Figures 2 and 6), cells were processed for TIRF microscopy, Tfn internalization, or immunoblotting.

Cell lysates and immunoblotting were done as previously described (Antonescu *et al.*, 2010), using the following antibodies: goat polyclonal anti-PIP5Kα (Santa Cruz Biotechnology, Santa Cruz, CA), rabbit polyclonal anti-GFP (The Schmid Lab at The Scripps Research Institute, La Jolla, CA) and TD-1, a mouse monoclonal anti-clathrin, which was a gift from Frances Brodsky (University of California, San Francisco, CA).

siRNA knockdown of PIP5K and Sjn1

Transfection of BSC-1 cells with siRNA duplexes was performed using HiPerFect (Qiagen, Chatsworth, CA) as per the manufacturer's instructions, and as previously described (Antonescu *et al.*, 2010). siRNA duplexes used were as follows: control siRNA was ON-TARGETplus nontargeting siRNA #1 (Dharmacon, Lafayette, CO), PIP5Kα (AAC TGC CGC GCT TCA AGA TAA; Qiagen), and Sjn1 (AAT GAC AAA GCT CGA GCA CTT; Qiagen). Transfection of cells with cDNAs was performed using Lipofectamine 2000 (Invitrogen, Carlsbad, CA), as per the manufacturer's instructions, as previously described (Antonescu *et al.*, 2010). For dual-color, time-lapse TIRF microscopy experiments, cells expressing the lowest detectable levels of each mCherry-tagged PIP5K and 5′-inositol phosphatase were selected for imaging.

To detect mRNA levels following siRNA-mediated knockdown, real-time quantitative PCR experiments were performed using a Chromo4 DNA Engine (Bio-Rad, Hercules, CA) as previously described (Antonescu *et al.*, 2010). Specific primers for each of PIP5Kα (forward: CTG TTG CCT TCC GCT ACT TC; reverse: AAA GTC GGG TTC TGG TT) and Sjn1 (forward: GAG GCC ATT GAT GTT TTG CT; reverse: CTT CCC ACC ATT CAC ATT CC) were designed using Primer3 software (Rozen and Skaletsky, 2000). For determination of the relative amounts of mRNA in each sample, all conditions are expressed as a percentage of mRNA detected in control siRNA-treated cells.

Live-cell TIRF microscopy and CCP lifetime analysis

TIRF mictroscopy was performed using a 100 × 1.49 NA CFI Apo TIRF objective (Nikon) mounted on a Ti-Eclipse inverted microscope with Perfect Focus System option (Nikon). Imaging was performed on cells incubated in DMEM lacking phenol red and supplemented with 3% fetal calf serum. Time-lapse image sequences from different cells were acquired at either a 400 ms or 2 s frame rate using a CoolSNAP HQ2 monochrome CCD camera (Photometrics, Tuscon, AZ). Dual-channel, time-lapse image series were acquired by sequential, nearly simultaneous acquisition of individual channels, using 100- to 150-ms exposures for each at an overall frame rate of 2 s. Fluorescent particle detection, lifetime tracking, and lifetime analysis of CCPs in BSC-1 cells stably expressing eGFP-CLC were performed as previously described and validated (Jaqaman *et al.*, 2008; Loerke *et al.*, 2009; Mettlen *et al.*, 2009). Intensity profile analysis on CCP lifetime cohorts was performed as previously described (Mettlen *et al.*, 2010; Loerke *et al.*, 2011) following normalization to background fluorescence.

In dual-channel movies, to distinguish between CCPs containing 5′-phosphatases and those without (see Supplemental Movie 8), we

tracked CCPs based on the eGFP-CLC signal in the "master" channel and classified CCPs based on the statistical significance of the fluorescence signal of the mCherry-tagged phosphatase in the "slave" channel at these sites. To establish the significance of the signal in the slave channel, we first determined, at each time point, whether the intensity value was above background level with confidence $\alpha = 0.95$. The intensity value was estimated by fitting a Gaussian approximation of the point-spread function to the slave channel signal at the CCP site. For the purpose of the statistical test, mean and variance of the background were estimated in a ring-shaped mask around the CCP, excluding all pixels with a significant signal at the CCP. Next we counted the number k of time points with a significant signal in a CCP track and tested whether $k > k_t$, where the threshold k_t is derived from the binomial cumulative distribution function $B(k_t;n,p) \geq 0.95$, where n is the total number of time points covered by the CCP track, and p is the probability for a signal to be significant by chance. The value of p was determined by computing the fraction of pixels in a Gaussian-filtered image of the endocytically active zones that are above background with a confidence level $\alpha = 0.95$. Endocytically active zones were defined expanding the islands of pixels belonging to the detected CCPs by five pixels in all directions, using a morphological dilution operator.

Statistical analyses

Differences in CCP subpopulation lifetimes and percent contribution among various treatments were determined following a jackknife analysis of parameter uncertainty described previously (Mettlen *et al.*, 2009). Statistical analyses of differences among initiation density measurements were performed with the Mann–Whitney rank sum test, with $p < 0.05$ as a threshold for significant difference among conditions. Measurements of Tfn uptake were subjected to analysis of variance with Neumann–Keuls posttest, with $p < 0.05$ as a threshold for significant difference among conditions. Measurements of maximum eGFP-CLC fluorescence intensity within CCP tracks and mRNA and protein levels were subjected to Student's *t* test, with $p < 0.05$ as a threshold for significant difference among conditions.

ACKNOWLEDGMENTS

We thank Marcel Mettlen, Allen Liu, and Sylvia Neumann for critical reading of this manuscript and helpful discussions and Don Hilgemann for helpful discussions. We also thank Vasyl Lukiyanchuk for technical assistance and Daniel Nuñez and Dinah Loerke for early quantification of CCP intensity and initiation. This work was supported by National Institutes of Health grants GM73165 (to G.D. and S.L.S.) and MH61345 (to S.L.S.) and by a Swiss National Science Foundation fellowship (to F.A.). This is TSRI Ms. No: 21104.

REFERENCES

Abe N, Inoue T, Galvez T, Klein L, Meyer T (2008). Dissecting the role of PtdIns(4,5)P2 in endocytosis and recycling of the transferrin receptor. J Cell Sci 121, 1488–1494.

Antonescu CN, Danuser G, Schmid SL (2010). Phosphatidic acid plays a regulatory role in clathrin-mediated endocytosis. Mol Biol Cell 21, 2944–2952.

Bairstow SF, Ling K, Su X, Firestone AJ, Carbonara C, Anderson RA (2006). Type Iγ661 phosphatidylinositol phosphate kinase directly interacts with AP2 and regulates endocytosis. J Biol Chem 281, 20632–20642.

Barbieri MA, Heath CM, Peters EM, Wells A, Davis JN, Stahl PD (2001). Phosphatidylinositol-4-phosphate 5-kinase-1beta is essential for epidermal growth factor receptor-mediated endocytosis. J Biol Chem 276, 47212–47216.

Botelho RJ, Teruel M, Dierckman R, Anderson R, Wells A, York JD, Meyer T, Grinstein S (2000). Localized biphasic changes in phosphatidylinositol-4,5-bisphosphate at sites of phagocytosis. J Cell Biol 151, 1353–1368.

Carlton JG, Cullen PJ (2005). Coincidence detection in phosphoinositide signaling. Trends Cell Biol 15, 540–547.

Catimel B, Schieber C, Condron M, Patsiouras H, Connolly L, Catimel J, Nice EC, Burgess AW, Holmes AB (2008). The PI(3,5)P2 and PI(4,5)P2 interactomes. J Proteome Res 7, 5295–5313.

Chang-Ileto B, Frere SG, Chan RB, Voronov SV, Roux A, Di Paolo G (2011). Synaptojanin 1-mediated PI(4,5)P_2 hydrolysis is modulated by membrane curvature and facilitates membrane fission. Dev Cell 20, 206–218.

Choudhury R, Noakes CJ, McKenzie E, Kox C, Lowe M (2009). Differential clathrin binding and subcellular localization of OCRL1 splice isoforms. J Biol Chem 284, 9965–9973.

Conner SD, Schmid SL (2003). Regulated portals of entry into the cell. Nature 422, 37–44.

Cremona O *et al.* (1999). Essential role of phosphoinositide metabolism in synaptic vesicle recycling. Cell 99, 179–188.

Di Paolo G, Pellegrini L, Letinic K, Cestra G, Zoncu R, Voronov S, Chang S, Guo J, Wenk MR, De Camilli P (2002). Recruitment and regulation of phosphatidylinositol phosphate kinase type 1 gamma by the FERM domain of talin. Nature 420, 85–89.

Doughman RL, Firestone AJ, Anderson RA (2003). Phosphatidylinositol phosphate kinases put PI4,5P(2) in its place. J Membr Biol 194, 77–89.

Ehrlich M, Boll W, Van Oijen A, Hariharan R, Chandran K, Nibert ML, Kirchhausen T (2004). Endocytosis by random initiation and stabilization of clathrin-coated pits. Cell 118, 591–605.

Ford MG, Pearse BM, Higgins MK, Vallis Y, Owen DJ, Gibson A, Hopkins CR, Evans PR, McMahon HT (2001). Simultaneous binding of PtdIns(4,5)P2 and clathrin by AP180 in the nucleation of clathrin lattices on membranes. Science 291, 1051–1055.

Fujita A, Cheng J, Tauchi-Sato K, Takenawa T, Fujimoto T (2009). A distinct pool of phosphatidylinositol 4,5-bisphosphate in caveolae revealed by a nanoscale labeling technique. Proc Natl Acad Sci USA 106, 9256–9261.

Gaidarov I, Keen JH (1999). Phosphoinositide-AP-2 interactions required for targeting to plasma membrane clathrin-coated pits. J Cell Biol 146, 755–764.

Harris TW, Hartwieg E, Horvitz HR, Jorgensen EM (2000). Mutations in synaptojanin disrupt synaptic vesicle recycling. J Cell Biol 150, 589–600.

Haucke V (2005). Phosphoinositide regulation of clathrin-mediated endocytosis. Biochem Soc Trans 33, 1285–1289.

Henne WM, Boucrot E, Meinecke M, Evergren E, Vallis Y, Mittal R, McMahon HT (2010). FCHo proteins are nucleators of clathrin-mediated endocytosis. Science 328, 1281–1284.

Itoh T, Koshiba S, Kigawa T, Kikuchi A, Yokoyama S, Takenawa T (2001). Role of the ENTH domain in phosphatidylinositol-4,5-bisphosphate binding and endocytosis. Science 291, 1047–1051.

Jackson LP, Kelly BT, McCoy AJ, Gaffry T, James LC, Collins BM, Höning S, Evans PR, Owen DJ (2010). A large-scale conformational change couples membrane recruitment to cargo binding in the AP2 clathrin adaptor complex. Cell 141, 1220–1229.

Jaqaman K, Loerke D, Mettlen M, Kuwata H, Grinstein S, Schmid SL, Danuser G (2008). Robust single-particle tracking in live-cell time-lapse sequences. Nat Methods 5, 695–702.

Jost M, Simpson F, Kavran JM, Lemmon MA, Schmid SL (1998). Phosphatidylinositol-4,5-bisphosphate is required for endocytic coated vesicle formation. Curr Biol 8, 1399–1402.

Kahlfeldt N, Vahedi-Faridi A, Koo SJ, Schäfer JG, Krainer G, Keller S, Saenger W, Krauss M, Haucke V (2010). Molecular basis for association of PIPKIγ-p90 with clathrin adaptor AP-2. J Biol Chem 285, 2734–2749.

Kim WT, Chang S, Daniell L, Cremona O, Di Paolo G, De Camilli P (2002). Delayed reentry of recycling vesicles into the fusion-competent synaptic vesicle pool in synaptojanin 1 knockout mice. Proc Natl Acad Sci USA 99, 17143–17148.

Krauss M, Kukhtina V, Pechstein A, Haucke V (2006). Stimulation of phosphatidylinositol kinase type I-mediated phosphatidylinositol (4,5)-bisphosphate synthesis by AP-2mu-cargo complexes. Proc Natl Acad Sci USA 103, 11934–11939.

Liu AP, Aguet F, Danuser G, Schmid SL (2010). Local clustering of transferrin receptors promotes clathrin-coated pit initiation. J Cell Biol 191, 1381–1393.

Liu J, Sun Y, Drubin DG, Oster GF (2009). The mechanochemistry of endocytosis. PLoS Biol 7, e1000204.

Loerke D, Mettlen M, Schmid SL, Danuser G (2011). Measuring the hierarchy of molecular events during clathrin-mediated endocytosis. Traffic 12, 815–825.

Loerke D, Mettlen M, Yarar D, Jaqaman K, Jaqaman H, Danuser G, Schmid SL (2009). Cargo and dynamin regulate clathrin-coated pit maturation. PLoS Biol 7, 3e57.
Malecz N, McCabe PC, Spaargaren C, Qiu R, Chuang Y, Symons M (2000). Synaptojanin 2, a novel Rac1 effector that regulates clathrin-mediated endocytosis. Curr Biol 10, 1383–1386.
Mao Y, Balkin DM, Zoncu R, Erdmann KS, Tomasini L, Hu F, Jin MM, Hodsdon ME, De Camilli P (2009). A PH domain within OCRL bridges clathrin-mediated membrane trafficking to phosphoinositide metabolism. EMBO J 28, 1831–1842.
McLaughlin S, Wang J, Gambhir A, Murray D (2002). PIP(2) and proteins: interactions, organization, and information flow. Annu Rev Biophys Biomol Struct 31, 151–175.
Merrifield CJ, Perrais D, Zenisek D (2005). Coupling between clathrin-coated-pit invagination, cortactin recruitment, and membrane scission observed in live cells. Cell 121, 593–606.
Mettlen M, Loerke D, Yarar D, Danuser G, Schmid SL (2010). Cargo- and adaptor-specific mechanisms regulate clathrin-mediated endocytosis. J Cell Biol 188, 919–933.
Mettlen M, Stoeber M, Loerke D, Antonescu CN, Danuser G, Schmid SL (2009). Endocytic accessory proteins are functionally distinguished by their differential effects on the maturation of clathrin-coated pits. Mol Biol Cell 20, 3251–3260.
Nakano-Kobayashi A, Yamazaki M, Unoki T, Hongu T, Murata C, Taguchi R, Katada T, Frohman MA, Yokozeki T, Kabaho Y (2007). Role of activation of PIP5Kgamma661 by AP-2 complex in synaptic vesicle endocytosis. EMBO J 26, 1105–1116.
Nakatsu F, Perera RM, Lucast L, Zoncu R, Domin J, Gertler FB, Toomre D, De Camilli P (2010). The inositol 5-phosphatase SHIP2 regulates endocytic clathrin-coated pit dynamics. J Cell Biol 190, 307–315.
Padron D, Wang YJ, Yamamoto M, Yin H, Roth MG (2003). Phosphatidylinositol phosphate 5-kinase Ibeta recruits AP-2 to the plasma membrane and regulates rates of constitutive endocytosis. J Cell Biol 162, 693–701.
Perera RM, Zoncu R, Lucast L, De Camilli P, Toomre D (2006). Two synaptojanin 1 isoforms are recruited to clathrin-coated pits at different stages. Proc Natl Acad Sci USA 103, 19332–19337.
Praefcke GJK, Ford MGJ, Schmid E M, Olesen LE, Gallop JL, Peak-Chew S-Y, Vallis Y, Babu MM, Mills IG, McMahon HT (2004). Evolving nature of the AP2 alpha-appendage hub during clathrin-coated vesicle endocytosis. EMBO J 23, 4371–4383.
Rappoport JZ, Kemal S, Benmerah A, Simon SM (2006). Dynamics of clathrin and adaptor proteins during endocytosis. Am J Physiol Cell Phys 291, C1072–C1081.
Rozen S, Skaletsky H (2000). Primer3 on the WWW for general users and for biologist programmers. Methods Mol Biol 132, 365–386.
Rusk N, Le PU, Mariggio S, Guay G, Lurisci C, Nabi IR, Corda D, Symons M. (2003). Synaptojanin 2 functions at an early step of clathrin-mediated endocytosis. Curr Biol 13, 659–663.
Saffarian S, Kirchhausen T (2008). Differential evanescence nanometry: live-cell fluorescence measurements with 10-nm axial resolution on the plasma membrane. Biophys J 94, 2333–2342.
Schmid EM, Ford MGJ, Burtey A, Praefcke GJK, Peak-Chew SY, Mills IG, Benmerah A, McMahon HT (2006). Role of the AP2 beta-appendage hub in recruiting partners for clathrin-coated vesicle assembly. PLoS Biol 4, e262.
Schmid EM, McMahon HT (2007). Integrating molecular and network biology to decode endocytosis. Nature 448, 883–888.
Sigismund S, Argenzio E, Tosoni D, Cavallaro E, Polo S, Di Fiore PP (2008). Clathrin-mediated internalization is essential for sustained EGFR signaling but dispensable for degradation. Dev Cell 15, 209–219.
Slepnev VI, De Camilli P (2000). Accessory factors in clathrin-dependent synaptic vesicle endocytosis. Nat Rev Neurosci 1, 161–172.
Sun Y, Carroll S, Kaksonen M, Toshima JY, Drubin DG (2007). PtdIns(4,5)P2 turnover is required for multiple stages during clathrin- and actin-dependent endocytic internalization. J Cell Biol 177, 355–367.
Taylor MJ, Perrais D, Merrifield CJ (2011). A high precision survey of the molecular dynamics of Mammalian clathrin-mediated endocytosis. PLoS Biol 9, e1000604.
Thieman JR, Mishra SK, Ling K, Doray B, Anderson RA, Traub LM (2009). Clathrin regulates the association of PIPKIgamma661 with the AP-2 adaptor beta2 appendage. J Biol Chem 284, 13924–13939.
Traub LM (2003). Sorting it out: AP-2 and alternate clathrin adaptors in endocytic cargo selection. J Cell Biol 163, 203–208.
Vallis Y, Wigge P, Marks B, Evans PR, McMahon HT (1999). Importance of the pleckstrin homology domain of dynamin in clathrin-mediated endocytosis. Curr Biol 9, 257–260.
Wenk MR, Pellegrini L, Klenchin VA, Di Paolo G, Chang S, Daniell L, Arioka Mm, Martin TF, De Camilli P (2001). PIP kinase Igamma is the major PI(4,5)P(2) synthesizing enzyme at the synapse. Neuron 32, 79–88.
Wong R, Hadjiyanni I, Wei H-C, Polevoy G, McBride R, Sem KP, Brill JA (2005). PIP2 hydrolysis and calcium release are required for cytokinesis in Drosophila spermatocytes. Curr Biol 15, 1401–1406.
Yarar D, Surka MC, Leonard MC, Schmid SL (2008). SNX9 activities are regulated by multiple phosphoinositides through both PX and BAR domains. Traffic 9, 133–46.
Yarar D, Waterman-Storer CM, Schmid SL (2007). SNX9 couples actin assembly to phosphoinositide signals and is required for membrane remodeling during endocytosis. Dev Cell 13, 43–56.
Yun M, Keshvara L, Park CG, Zhang YM, Dickerson JB, Zheng J, Rock CO, Curran T, Park HW (2003). Crystal structures of the Dab homology domains of mouse disabled 1 and 2. J Biol Chem 278, 36572–36581.
Zoncu R, Perera RM, Sebastian R, Nakatsu F, Chen H, Balla T, Ayala G, Toomre D, De Camilli PV (2007). Loss of endocytic clathrin-coated pits upon acute depletion of phosphatidylinositol 4,5-bisphosphate. Proc Natl Acad Sci USA 104, 3793–3798.